

This is a repository copy of *Two high-risk susceptibility loci at 6p25.3 and 14q32.13 for Waldenström macroglobulinemia.*

White Rose Research Online URL for this paper:

<https://eprints.whiterose.ac.uk/137909/>

Version: Published Version

Article:

McMaster, Mary L, Berndt, Sonja I, Zhang, Jianqing et al. (78 more authors) (2018) Two high-risk susceptibility loci at 6p25.3 and 14q32.13 for Waldenström macroglobulinemia. Nature Communications. 4182. ISSN 2041-1723

<https://doi.org/10.1038/s41467-018-06541-2>

Reuse

This article is distributed under the terms of the Creative Commons Attribution (CC BY) licence. This licence allows you to distribute, remix, tweak, and build upon the work, even commercially, as long as you credit the authors for the original work. More information and the full terms of the licence here:

<https://creativecommons.org/licenses/>

Takedown

If you consider content in White Rose Research Online to be in breach of UK law, please notify us by emailing eprints@whiterose.ac.uk including the URL of the record and the reason for the withdrawal request.

ARTICLE

DOI: 10.1038/s41467-018-06541-2

OPEN

Two high-risk susceptibility loci at 6p25.3 and 14q32.13 for Waldenström macroglobulinemia

Mary L. McMaster et al.[#]

Waldenström macroglobulinemia (WM)/lymphoplasmacytic lymphoma (LPL) is a rare, chronic B-cell lymphoma with high heritability. We conduct a two-stage genome-wide association study of WM/LPL in 530 unrelated cases and 4362 controls of European ancestry and identify two high-risk loci associated with WM/LPL at 6p25.3 (rs116446171, near *EXOC2* and *IRF4*; OR = 21.14, 95% CI: 14.40–31.03, $P = 1.36 \times 10^{-54}$) and 14q32.13 (rs117410836, near *TCL1*; OR = 4.90, 95% CI: 3.45–6.96, $P = 8.75 \times 10^{-19}$). Both risk alleles are observed at a low frequency among controls (~2–3%) and occur in excess in affected cases within families. In silico data suggest that rs116446171 may have functional importance, and in functional studies, we demonstrate increased reporter transcription and proliferation in cells transduced with the 6p25.3 risk allele. Although further studies are needed to fully elucidate underlying biological mechanisms, together these loci explain 4% of the familial risk and provide insights into genetic susceptibility to this malignancy.

Correspondence and requests for materials should be addressed to M.L.M. (email: Mary.McMaster@nih.hhs.gov). [#]A full list of authors and their affiliations appears at the end of the paper.

Waldenström macroglobulinemia (WM) is a subset of lymphoplasmacytic lymphoma (LPL) characterized by the presence of an immunoglobulin type M (IgM) monoclonal gammopathy¹. Together, WM/LPL account for 2% of all non-Hodgkin lymphoma, with an estimated 2330 new cases diagnosed per year in the US². Family history of WM/LPL or related lymphoproliferative disorder is strongly associated with WM/LPL risk^{3,4}. Autoimmunity and select infections are also associated with WM/LPL risk^{5–8}, and limited data suggest a possible relationship with certain lifestyle and occupational factors⁸, but overall little is known about its etiology. A somatic driver mutation, *MYD88* p.L265P, occurs in most cases of WM⁹. However, germline *MYD88* (myeloid differentiation primary response 88) mutations have not been observed, and despite early promising findings by linkage analysis¹⁰, no predisposing gene mutations have been conclusively reported to date. Characterizing the genetic factors influencing susceptibility to WM/LPL is an important step toward understanding its etiology. To discover genetic loci for WM/LPL susceptibility, we perform a two-stage genome-wide association study (GWAS) of WM/LPL, leveraging a family-based oversampling approach in the discovery followed by replication in an independent, predominantly non-familial, cohort. Here we report new susceptibility loci at 6p25.3 and 14q32.13 for WM/LPL and provide insights into the genetic etiology of this distinctive B-cell lymphoma.

Results

Discovery population, genotyping, and analysis. Oversampling cases with a family history of hematological malignancy, we genotyped 244 WM/LPL cases of European descent (Supplementary Table 1), including 98 unrelated cases (40%) from high-risk families, using the Illumina OmniExpress SNP microarray chip and selected controls previously genotyped on the OmniExpress or Omni2.5^{11,12}. Following application of rigorous quality-control metrics, data for 603,492 SNPs with minor allele frequency (MAF) >1% in 217 unrelated cases and 3798 controls of European ancestry remained for analysis (Methods, Supplementary Table 2). A quantile–quantile plot of the association results with genotyped SNPs, adjusted for age, sex, and principal components, revealed enrichment of small *P*-values based on a log-additive genetic model and a small degree of over-dispersion ($\lambda = 1.05$), consistent with other GWAS and due in part to possible polygenic effects¹³ (Supplementary Fig. 1a). Several SNPs at chromosome 6p25.3 reached genome-wide significance with *P*-values between 1.22×10^{-8} and 5.64×10^{-20} (Supplementary Fig. 2a).

To refine the association signal and identify other regions potentially associated with risk, we imputed common SNPs using the Haplotype Reference Consortium panel¹⁴. Following imputation and association testing (Supplementary Fig. 1b), the strongest association at 6p25.3 was rs116446171 ($P = 1.59 \times 10^{-48}$; information score = 0.9985; Supplementary Fig. 2b), a well-imputed SNP between *EXOC2* (Exocyst complex component 2, also known as *Sec5*) and *IRF4* (Interferon regulatory factor 4). A second SNP, rs76106586, was highly significant and in strong linkage disequilibrium (LD; $r^2 = 1.0$) with rs116446171. Although other SNPs appeared to be strongly associated with risk, conditional association analyses suggest a single signal accounted for the association in this region (Supplementary Table 3). SNPs at chromosome 14q32.13 also reached genome-wide significance, and conditional analyses suggest there may be more than one independent signal at 14q32.13 (Supplementary Fig. 2b; Supplementary Tables 4, 5).

Independent replication without familial enrichment. Eleven SNPs (Supplementary Table 6) with $P \leq 5 \times 10^{-6}$ in the discovery

analyses were selected for de novo replication in an additional 313 WM/LPL cases, with 24 (8%) reporting a positive family history, and 564 controls of European ancestry (Supplementary Tables 1, 2). The combined analysis of 530 WM/LPL cases and 4362 controls confirmed two distinct loci at chromosome 6p25.3 (rs116446171; odds ratio (OR) = 21.14, 95% confidence interval (CI) = 14.40–31.03, $P = 1.36 \times 10^{-54}$) and 14q32.13 (rs117410836, OR = 4.90, 95% CI = 3.45–6.96, $P = 8.75 \times 10^{-19}$), as shown in Table 1 and Fig. 1. Both SNPs were well-imputed in the discovery (information scores >0.96), and technical validation using Taqman or Sanger sequencing showed >99% concordance between imputed and genotyped calls for both SNPs (Supplementary Table 7). The SNPs were genotyped using two different genotyping platforms in the replication, suggesting that our results are not due to platform artifact. Although the effect estimates were attenuated in the replication, suggesting some inflation due to winner's curse and/or oversampling of familial cases in the discovery, both SNPs replicated with highly statistically significant *P*-values ($P = 2.54 \times 10^{-13}$ and 1.16×10^{-5} for rs116446171 and rs117410836, respectively; Table 1). The effects were similar when the analysis was limited to WM cases (rs116446171: OR = 24.41, 95% CI = 16.46–36.23, $P = 7.43 \times 10^{-57}$; rs117410836: OR = 5.14, 95% CI = 3.56–7.43, $P = 2.78 \times 10^{-18}$; Supplementary Table 6). A suggestive second independent signal was observed at 14q32.13 with a directly genotyped SNP (rs179159, $r^2 = 0.002$, $P = 4.66 \times 10^{-7}$; Supplementary Table 6), which was slightly attenuated after conditioning on rs117410836 ($P = 3.16 \times 10^{-6}$). No other locus replicated.

Risk-variant enrichment in WM/LPL families and heritability.

To assess whether the risk variants occurred at a higher than expected frequency within high-risk families, we genotyped the two loci in available affected relatives of familial cases. In families in which the index case had the rs116446171 risk variant, 76% of first-degree relatives with WM or its precursor, IgM monoclonal gammopathy of undetermined significance (MGUS), also carried the risk variant (Supplementary Table 8). Similarly, in families in which the index case had the rs117410836 risk variant, 86% of first-degree relatives with WM or IgM MGUS also carried the risk variant. In both instances, the risk variant frequency in affected relatives exceeded the expected 50% distribution ($P_{\text{binomial}} = 0.01$ for rs116446171 and $P_{\text{binomial}} = 0.03$ for rs117410836), which is consistent with theoretical models of familial co-segregation¹⁵. Exploration of heritability in a broader sense, using effect estimated from the replication, indicated that these two loci explain 4% of the familial risk for WM/LPL. When we explored the potential contribution of all common variants to the heritability, we estimated that common SNPs could explain ~25% (95% CI = 15.4–34.5%) of the heritability as a whole, suggesting more common loci are likely to be discovered with larger sample sizes.

Functional annotation of rs116446171. rs116446171 is located 679 base pairs (bp) downstream of the 3' untranslated region (UTR) of *EXOC2*, in a region bounded proximally by *IRF4* and *DUSP22* (Dual specificity phosphatase 22) and distally by *EXOC2* (Fig. 2a). To determine whether rs116446171 might be a functional susceptibility variant, we performed in silico analyses that indicated the SNP is located in a region overlapping enhancer histone marks, histone H3 lysine 4 mono-methylation (H3K4me1) and lysine 27 acetylation (H3K27ac), in B-lymphoblastoid cell lines (Supplementary Fig. 3). Analysis of promoter capture Hi-C data¹⁶ showed that this region interacts with the *IRF4* and, to a lesser extent, *DUSP22* promoters in naïve and total primary B-cells (Supplementary Fig. 3), consistent with reports of long-range enhancer-promoter interactions^{17,18}. In

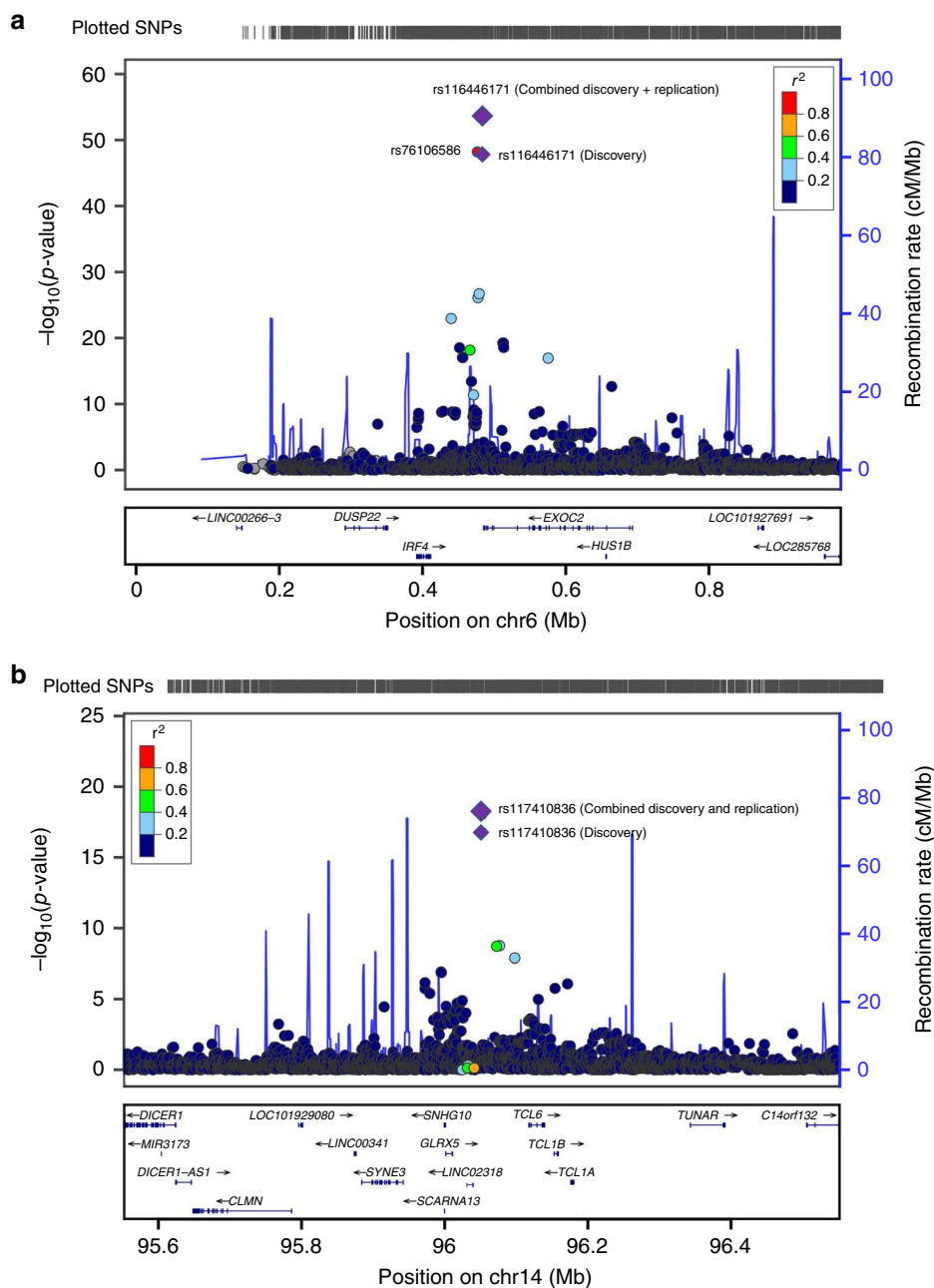


Fig. 1 Regional association plots of two SNPs associated with the risk of WM/LPL. **a** Chromosome 6p25.3 (rs116446171) and **b** chromosome 14q32.13 (rs117410836). Shown are the $-\log_{10}$ association P -values from the discovery log-additive genetic model for all SNPs in the region (dots) and combined discovery and replication fixed-effects analysis (diamonds). The lead SNPs are shown in purple, with results from both the discovery (small diamonds) and combined (large diamonds) analyses. Estimated recombination rates (from 1000 Genomes) are plotted in blue. The SNPs surrounding the most significant SNP are color-coded to reflect their correlation with this SNP. Pairwise r^2 values are from 1000 Genomes European data. Locations of recombination hotspots are depicted by peaks corresponding to the rate of recombination. Genes, position of exons and direction of exons and direction of transcription from UCSC genome browser (<http://genome.ucsc.edu>) are denoted. Plots were generated using LocusZoom (<http://csg.sph.umich.edu/locuszoom>)

silico analyses indicated that the rs116446171 (C) allele (“wild type”) is a predicted binding site for microRNA (miR) miR-378a-5p, and the single-nucleotide change from wild type (C) to risk (G) variant converts the nucleotide sequence to a binding site for a different miR, miR-324-3p (Fig. 2b).

No evidence for significant *cis*-eQTLs (expression quantitative trait loci) within Epstein-Barr virus (EBV)-transformed lymphocytes or whole blood was observed from analysis of Genotype-Tissue Expression Project (GTEx) data (Supplementary Table 9).

rs116446171 is not located within the 3’UTR of the annotated transcript of *EXOC2*; however, alternative cleavage and polyadenylation has known capability to alter the length of 3’UTR regions¹⁹. Cell-type-specific polyadenylation occurs in the immunoglobulin locus and mature B-cells, resulting in transcript isoforms that lead to changes in protein structure²⁰. Therefore, we explored in silico data for evidence for an extended UTR for *EXOC2* (Supplementary Fig. 4). Based on published 3’ end-sequencing data performed by various groups^{20–22}, we found evidence that rs116446171 could be

Table 1 Association statistics for two independent SNP genotypes and WM/LPL risk

Nearest gene	SNP	Position ^a	Variant Eff ^b /Oth	Stage	EAF controls	Cases/controls n/n	OR	(95% CI)	P-value
6p25.3 EXOC2	rs116446171	484453	G/C	Stage 1	0.0191	217/3798	56.44	(32.89, 96.85)	1.59E-48
				Stage 2	0.0195	312/564	7.71	(4.46, 13.33)	2.54E-13
				Combined		529/4362	21.14	(14.40, 31.03)	1.36E-54
14q32.13 Intergenic	rs117410836	96051974	C/T	Stage 1	0.0266	217/3798	10.62	(6.17, 18.29)	1.63E-17
				Stage 2	0.0355	306/563	2.81	(1.77, 4.45)	1.16E-05
				Combined		523/4361	4.90	(3.45, 6.96)	8.75E-19

For stages 1 and 2, P-values were generated using logistic regression. For the combined stage, the odds ratio and P-values were generated using a fixed-effects model controlling for age, gender and genotyping center
 WM Waldenström macroglobulinemia, LPL lymphoplasmacytic lymphoma, SNP single-nucleotide polymorphism, Eff effect, Oth other, EAF effect allele frequency, n number, OR odds ratio, CI confidence interval
^aGenome coordinates are from NCBI human genome GRCh37/human genome (hg) build 19
^bVariant associated with an effect on risk of WM/LPL

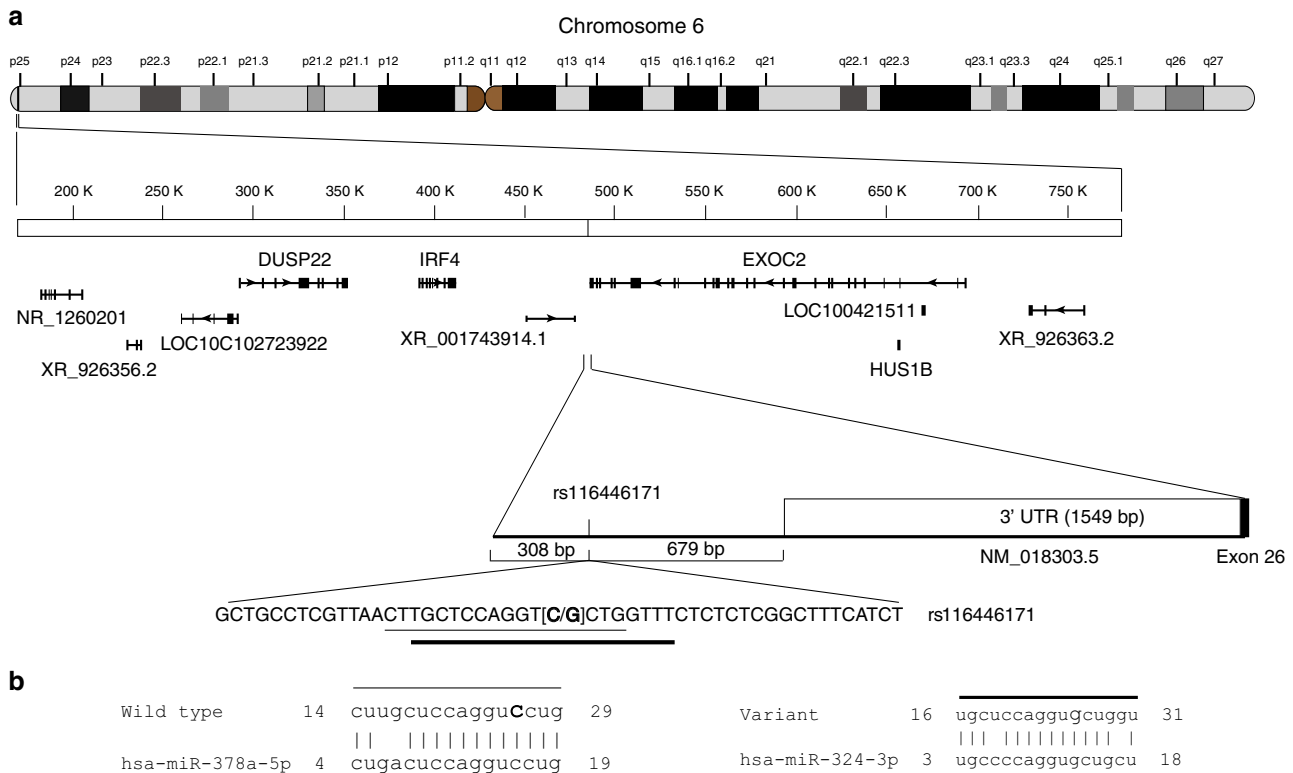


Fig. 2 Genomic position and alignments of rs116446171 to miRs. **a** Schematic representation of the position of rs116446171 relative to the 3'UTR of EXOC2 on chromosome 6 and **b** alignments of rs116446171 wild type and risk variants with the binding sites of microRNAs, miR-378a-5p and miR-324-3p

an enhancer in normal and malignant B-cells as well as other cell types. We then determined whether the SNP can cause changes to the secondary structure of the RNA of EXOC2, using RNAfold Webservice²³ to predict in silico the centroid model with minimum free energy structures and base pair probabilities in the region surrounding rs116446171. As shown in Supplementary Fig. 5, the risk variant is predicted to induce a bulge in the region compared to the other variant. Data from cBioPortal²⁴ and COSMIC²⁵ for the closest gene, EXOC2, indicated a low frequency of somatic mutations in hematopoietic and lymphoid tissues, suggesting that occurrence of age-dependent clonal somatic mosaicism is unlikely to account for our results.

In vitro functional evaluation of rs116446171. To further explore the functional role of the rs116446171 risk variant, we

used an enhanced green fluorescent protein (EGFP) reporter assay to estimate transcript levels. In addition to the pCS-EGFP-3'G (risk) construct, we also created pCS-EGFP-3'C (wild type, WT) and pCS-EGFP-3'Δ (null) constructs to use as comparators. Stably transduced HEK293T cell lines were grown for conducting the assays. Cells transduced with the risk allele reporter pCS-EGFP-3'G showed significantly increased EGFP fluorescence compared to the WT, Null, and the commercial EGFP reporters (Fig. 3a). Quantitative PCR analysis showed significantly higher EGFP mRNA levels in cells harboring the risk variant (Fig. 3b), possibly resulting from increased transcription or translational controls such as stability of EGFP mRNA. Furthermore, cells harboring the Null construct had significantly decreased EGFP mRNA levels, suggesting the deleted segment of DNA harboring the SNP might have an important role in the self-maintenance of

transcriptional control of EGFP mRNA. We saw no effect on *EXOC2* transcript levels (Supplementary Fig. 6). Transduced cells harboring the risk variant showed significantly increased cell proliferation, based on the MTT assay (Methods), compared to cells transduced with the empty, wild type, or null vectors (Fig. 3c).

To evaluate the functional effect of the miR-binding site conversion conferred by the risk variant, we created pre-microRNA expression plasmids and transfected cells containing the wild type (C) or risk (G) variant (Methods). Overexpression of either premiR-378a-5p and premiR-324-3p in cells harboring the wild type or the risk variant decreased EGFP protein fluorescence (Fig. 4). However, no miR-specific effects were observed in the transfected cells overexpressing miR-378a-5p or miR-324-3p, respectively (Supplementary Fig. 7), suggesting that the observed phenotypes in the cells harboring the risk variant might not be due to direct interference of the miRs with translation.

To further investigate the possible role of the miR-324-3p binding site created by the risk variant, we cloned 2, 4, or 8 tandem repeats of the 25-base pair (bp) sequence centered around rs116446171G/C into the 3'UTR of the EGFP reporter, in both *cis* and *trans* orientations (Methods). We observed a proportional increase in EGFP mRNA transcript levels (Fig. 5a) and a similar effect on cellular proliferation (Fig. 5b) from the constructs incorporating increasing numbers of repeats of the rs116446171 risk variant that appeared to be dose-dependent in *cis* but, as expected, not in *trans*. These data suggest rs116446171 alters a binding site for miRNA. The miR-324-3p binding site results in increased gene expression. Previous studies have shown that miRs can influence tumorigenesis through various processes^{26,27}. miR-324-3p induces promoter-mediated expression of RelA, a subunit of NF- κ B (nuclear factor kappa-light-chain-enhancer of activated B-cells)²⁸, and the NF- κ B signaling network is important in the pathogenesis of B-cell malignancies, including WM^{29,30}. However, the precise mechanism by which non-canonical miR binding might increase WM/LPL risk is unclear.

Functional annotation of rs117410836. The most significant SNP marker at 14q32.13 (rs117410836) is located near an uncharacterized long non-coding RNA (lncRNA; *LINC02318*), *GLRX5* (glutaredoxin 5), and members of the T-cell leukemia (TCL) gene family (*TCL1A*, *TCL1B*, and *TCL6*). rs117410836 resides in a repressive chromatin domain with histone H3 lysine 27 trimethylation (H3K27me3) (Supplementary Fig. 3). In silico analyses using Hi-C data suggest that the region containing a linked SNP (rs1150666963; $r^2 = 0.75$) interacts with the *TCL1A* promoter in total primary B-cells (Supplementary Fig. 3; Methods).

Discussion

In this study, we used a two-stage genome-wide approach to identify association between genetic variants and the risk of WM/LPL. We oversampled familial WM/LPL cases to enrich for potential susceptibility loci in our discovery stage and used an independent, predominantly non-familial sample to replicate our results. We found two loci at 6p25.3 and 14q32.13 associated with WM/LPL risk in individuals of European ancestry.

Definitive identification of the functional variants and genes remains a major challenge of GWAS. In this study, the most significant SNP, rs116446171 (6p25.3), is identical to that shown to be highly associated with diffuse large B-cell lymphoma in European and East Asian populations^{31,32}. While this observation is congruent with data supporting the co-aggregation of B-cell disorders, we cannot yet exclude the possibility that another

highly significant linked SNP, such as rs76106586, is responsible for the observed association.

rs116446171 is located in proximity to *EXOC2*, *IRF4*, and *DUSP22*. These genes and their associated transcriptional programs have been implicated in a variety of lymphoid cancers^{33–35} and are plausible WM/LPL susceptibility genes. *IRF4* expression is aberrantly downregulated in WM/LPL³⁶, specifically in the plasma cell compartment³⁷. *IRF4* has a critical role in plasma cell differentiation, class-switch recombination, and germinal center fate decisions³⁸, and negatively regulates Toll-like-receptor (TLR) signaling by binding MYD88³⁹. *DUSP22* modulates immune and inflammatory responses through regulation of MAPK (mitogen-activated protein kinase) signaling⁴⁰ and suppresses IL6/STAT3 (interleukin 6/signal transducer and activator of transcription)-mediated signaling⁴¹, an important MYD88-independent mechanism for WM cell growth and survival⁴². *EXOC2* interacts with Ral (RAS-like proto-oncogene) proteins at the nexus of viral exposure and host immune response⁴³ and is critical for cancer cell proliferation, invasion, and metastasis^{44,45}; it also interacts with NF- κ pathway constituent, TBK1 (TANK binding kinase 1) to promote tumor cell survival⁴⁶.

The susceptibility locus at 14q32.13, rs117410836, maps most closely to the previously uncharacterized lncRNA, *LINC02318*. lncRNA regulation of transcription, cytokine production and other cellular functions has been implicated in cancer⁴⁷ as well as in the development and function of the innate immune system. Specific lncRNAs influence gene expression programs, including the NF- κ B signaling pathway⁴⁸, interact with transcription factors⁴⁹, and have been shown to be induced via the canonical TLR pathway involving MYD88 and NF- κ B proteins⁵⁰. Among TCL family members in this region, *TCL1* has been shown to be aberrantly expressed in 73% of WM tumor samples⁵¹. Dysregulated *TCL1* expression in B-cells enhances cell proliferation and survival, leading to cell transformation and mature B-cell tumors through multiple effector mechanisms, including NF- κ B activation^{52–55}. Limited data are available regarding genetic variation in this region⁵⁶. Thus, additional work is needed to understand the functional implications of variation at this locus and its relationship to WM/LPL.

In conclusion, we performed a GWAS of WM/LPL and identified two independent loci that are associated with the risk of WM/LPL with substantially higher than expected estimated odds ratios for a GWAS of an adult cancer. It is remarkable that the effect size for 6p25.3 is substantively different for WM/LPL compared to other subtypes of NHL. The effect size was especially pronounced in our discovery, where we oversampled familial cases that are more likely to harbor disease variants, but remained highly significant in a predominantly non-familial replication set. The large effect size observed for rs116446171 in 6p25.3 near *IRF4*, *DUSP22*, and *EXOC2* and preliminary in silico and functional evidence suggest we may have discovered an important non-coding variant for WM risk. Familial co-segregation analyses are necessary to understand the implications for familial risk and any warranted clinical application. Additional functional and epidemiological studies are needed to clarify underlying biological mechanisms and to identify additional susceptibility loci that may influence disease risk.

Methods

Study approval. Each participating study obtained written informed consent from all participants and approval from its respective human subjects review committee, as follows: CPS-II: Emory University Institutional Review Board; ENGELA: IRB00003888—Comité d'Évaluation Éthique de l'Inserm IRB #1; EPIC: Imperial College London; EpiLymph: International Agency for Research on Cancer; HPFS: Harvard TH Chan School of Public Health Institutional Review Board; Iowa-Mayo SPORE: University of Iowa and Mayo Clinic Institutional Review Board; Mayo CC: Mayo Clinic Institutional Review Board; MSKCC: Memorial Sloan-Kettering

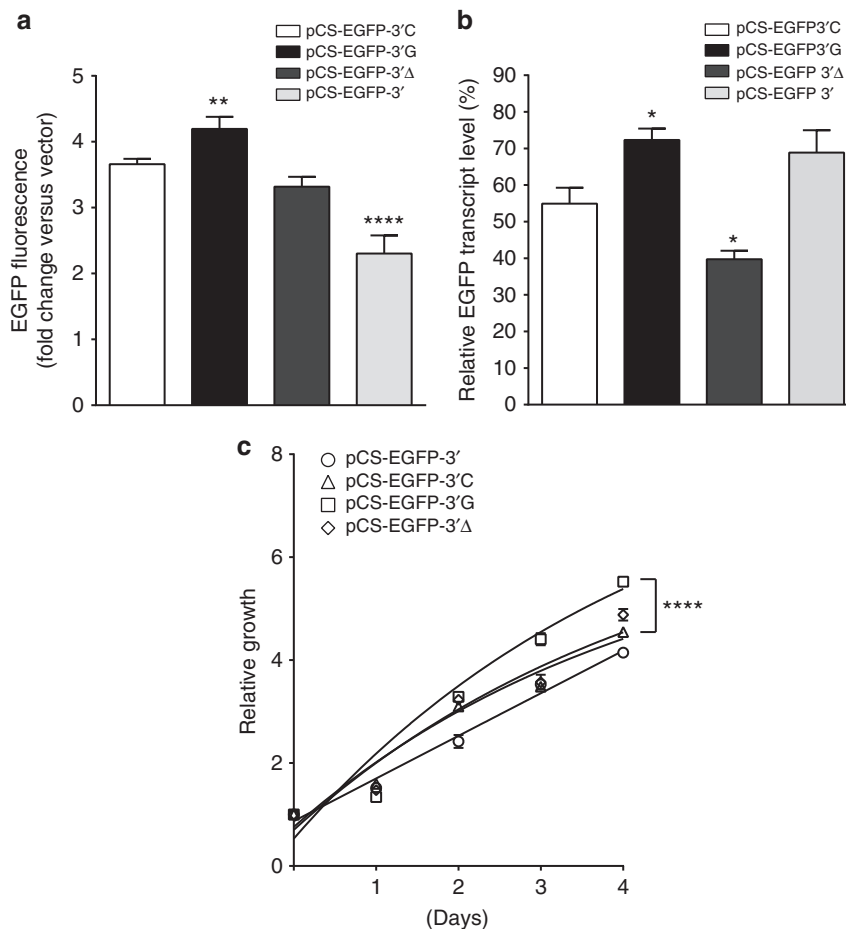


Fig. 3 The rs116446171 variants affect reporter activity and cell proliferation. **a** EGFP reporter activity in HEK293T stably transduced cell lines. Cells transduced with the risk variant (G) showed significantly increased fluorescence levels of EGFP compared to the cell lines transduced with the wild type (WT, C); $P = 0.012$. Cells transduced with the Null (Δ) had decreased EGFP fluorescence ($P = 0.054$, $n = 14$), and cells transduced with the commercial 3'UTR of *EXOC2* showed significantly decreased EGFP fluorescence ($P < 0.0001$, $n = 14$). Data are expressed as mean fold change relative to the cells transduced with the vector, \pm standard error of the mean (s.e.m.), $n = 14$ replicates. $**P < 0.01$, $****P < 0.0001$. **b** Quantitative PCR analysis of EGFP transcripts in HEK293T stably transduced cell lines. Significant changes of EGFP mRNA levels were detected in cells harboring the variant allele compared to the cells harboring the wild-type allele ($P = 0.031$). Cells harboring the Null allele had reduced EGFP transcripts levels ($P = 0.036$). Data are expressed as mean % change relative to the endogenous controls, \pm s.e.m., $n = 9$ replicates for each experiment. $*P < 0.05$. **c** Proliferation assay of cells harboring rs116446171, the deletion (Null) of an 18-bp segment centered on rs116446171, and the commercial 3'UTR reporter. The cell line transduced with the variant allele showed significantly increased cell proliferation compared to the cell lines transduced with the *EXOC2* 3'UTR, the WT and the Null. Data are expressed as mean fold change of the cell line in the day seeded, \pm s.e.m., $n = 9$ replicates. $****P < 0.0001$. All P -values were calculated with unpaired t -test

Cancer Center Institutional Review Board; NCI Family: NCI Clinical Center Institutional Review Board; NCI-SEER: NCI Special Studies Institutional Review Board; NHS: Partners Institutional Review Board/Brigham and Women's Hospital; NSW: NSW Cancer Council Ethics Committee; PLCO, NCI Special Studies Institutional Review Board; SCALE: Scientific Ethics Committee for the Capital Region of Denmark and Regional Ethical Review Board in Stockholm (Section 4) IRB#5; UCSF2: University of California San Francisco Committee on Human Research; WHI: Fred Hutchinson Cancer Research Center Institutional Review Board; Yale: Human Investigation Committee, Yale University School of Medicine (See Supplementary Table 1 for study abbreviations).

Phenotype definition. LPL was defined according to World Health Organization (WHO)^{1,57} criteria. WM was defined according to WHO^{1,57} and required the presence of both an LPL infiltrate in the bone marrow together with a monoclonal immunoglobulin type M (IgM) protein in the serum. In cases where histopathologic criteria for LPL were met but serum protein electrophoresis data were not available, the case was classified as LPL. Diagnoses were validated for all cases by medical and pathology reports. All cases were unrelated. Family history of WM/LPL or other B-cell malignancy (i.e., chronic lymphocytic leukemia (CLL), other non-Hodgkin lymphoma (NHL), Hodgkin lymphoma, or multiple myeloma) was ascertained by self-report, and positive family history was validated in a subset (83%).

Discovery population. Cases for the stage 1 discovery analysis included 207 participants in a WM family study at the National Cancer Institute (NCI Family)⁷ and 37 cases identified through a case-control study of NHL and CLL at the Mayo Clinic (Mayo CC). The 244 stage 1 cases included 98 reporting a family history of WM/LPL ($n = 42$) or other B-cell malignancy ($n = 56$), 118 cases reporting no family history, and 28 cases with unknown family history. Stage 1 controls ($n = 3812$) were obtained from a previous GWAS of NHL¹¹ and included 987 lymphoma-free controls from four US-based studies (National Cancer Institute—Surveillance, Epidemiology, and End Results Interdisciplinary Case-Control Study of Non-Hodgkin lymphoma (NCI-SEER); the Women's Health Initiative (WHI); a population-based case-control study in Connecticut women (Yale); and Mayo CC) and 2825 cancer-free controls from a study of prostate cancer in the Prostate, Lung, Colon, and Ovarian (PLCO) Cancer Screening Trial¹² (Supplementary Table 1). Characteristics of the discovery population are shown in Supplementary Table 2.

Discovery genotyping and quality control. All WM/LPL cases with sufficient DNA ($n = 244$) were genotyped on the Illumina OmniExpress SNP microarray chip at the NCI Cancer Genomics Research Laboratory (CGR). Genotypes were called using Illumina GenomeStudio software, and rigorous quality control metrics were employed to ensure that the resulting data were of high quality (Supplementary Table 10). All data analyses and management were conducted

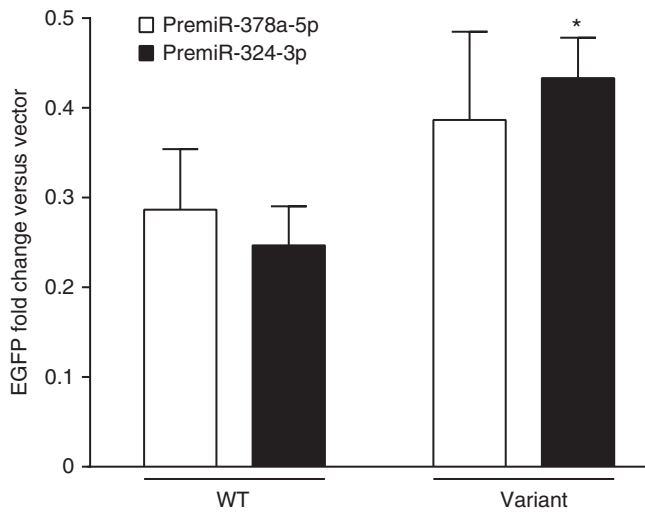


Fig. 4 EGFP reporter assay of interactions with microRNAs. Transient transfections with either the PremiR-378a-5p or PremiR-324-3p expression plasmid reduced the EGFP protein expression in cells harboring the wild type or variant allele equally (i.e., resulted in similar fold reductions). Transfection of PremiR-324-3p significantly increased the EGFP fluorescence in the cells harboring the variant allele compared to the wild type ($P = 0.040$). Data are expressed as mean fold change relative to the cells transfected with the pLV-miR vector, \pm s.e.m., $n = 9$ replicates. P -values were calculated with unpaired t -test. * $P < 0.05$. N.B. the scale of the fold change on the Y axis is < 1.0

using Genotyping Library and Utilities (GLU), version 1.0 (<http://code.google.com/p/glu-genetics/>). Specifically, we excluded 15 subjects at this step due to: samples with a call rate of $\leq 95\%$ (7 cases); insufficient phenotype data (5 cases); and unexpected duplicates ($>99.9\%$ concordance; 2 cases, 1 control). Quality control duplicates had $>99.9\%$ concordance. Genotype data from the controls were previously generated using the Illumina OmniExpress (Mayo CC, NCI-SEER, WHI, Yale) and the Illumina Omni2.5 (PLCO) chips and underwent the same quality control parameters as cases^{11,12}. We assessed ancestry using a set of population informative SNPs⁵⁸ and data from the HapMap CEU, YRI, and ASA populations. We estimated admixture coefficients for each sample using the GLU v1.0 struct.admix module based on the method by Pritchard et al.⁵⁹ and using HapMap⁶⁰ data as the fixed reference populations. Participants with $<80\%$ European ancestry were excluded (4 cases, 9 controls; Supplementary Fig. 8). One member of each related pair known to be within three degrees of relatedness by inspection of the pedigree or with estimated $\text{pihat} > 0.4$ was excluded (9 cases, 4 controls). After exclusions, all pairwise pihat estimates were < 0.08 for cases, and 217 cases and 3798 controls remained for analysis (Supplementary Table 10). For the analysis, SNPs with call rate $< 95\%$, Hardy-Weinberg equilibrium $P < 1 \times 10^{-6}$, minor allele frequency (MAF) $< 1\%$, or previously shown to be analytically uninformative were excluded, yielding 603,492 autosomal SNPs for analysis. To evaluate population substructure, we performed a principal components analysis using the GLU v1.0 struc.pca module, which is comparable to EIGENSTRAT⁶¹. Plots of the first 5 principal components are shown in Supplementary Fig. 9. We conducted initial association testing assuming a log-additive genetic model, adjusting for age, sex, and two principal components that were found to be significant in the null model.

Imputation of variants. To allow us to evaluate the genome more comprehensively for SNPs associated with WM, we imputed SNPs in the stage 1 discovery GWAS using the Michigan Imputation Server (<https://imputationserver.sph.umich.edu/index.html>) and the Haplotype Reference Consortium (HRCr1) panel (<https://www.sanger.ac.uk/science/collaboration/haplotype-reference-consortium>)¹⁴ following pre-phasing using SHAPEIT (https://mathgen.stats.ox.ac.uk/genetics_software/shapeit/shapeit.html#home). For imputation, SNPs with MAF $< 1\%$ were not excluded. Association testing on the imputed data was conducted using the Frequentist association module in SNPTEST v.2.5.2 (https://mathgen.stats.ox.ac.uk/genetics_software/snptest/snptest.html), assuming dosages for the genotypes, a log-additive model, and adjusting for age, sex and two significant principal components. Tested SNPs with MAF filter $< 2.5\%$ for cases and $< 1\%$ for controls or with SNPTEST INFO score filter < 0.3 were excluded, resulting in 6,440,053 autosomal SNPs.

Replication population. An independent stage 2 replication population included 313 WM/LPL cases from the NCI Family study ($n = 29$), Mayo CC/Iowa-Mayo

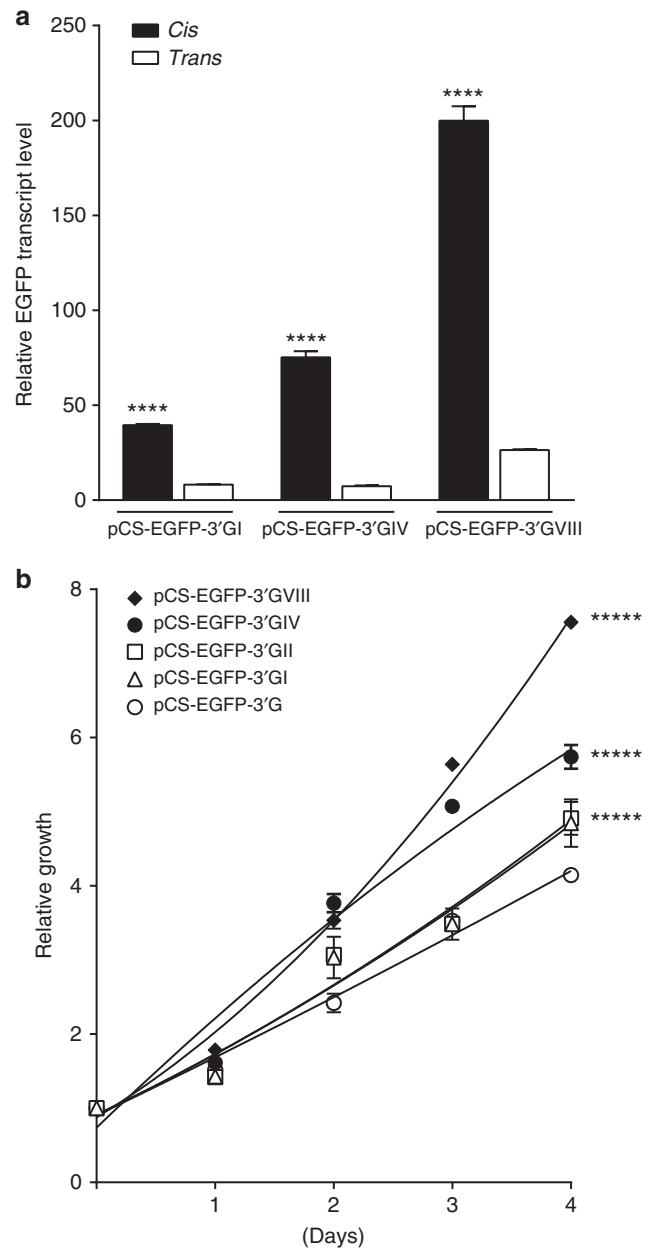


Fig. 5 Dose-dependent effect of rs116446171 variants on reporter transcription and cell proliferation. **a** Quantitative PCR analysis of EGFP transcripts in stably transduced cells with tandem repeats of the rs116446171 variant allele. The variant allele was inserted within the EXOC2 3'UTR region as a single copy or as two, four and eight repeats in either *cis* or *trans* orientation. Data are expressed as mean fold change of the endogenous controls, \pm s.e.m., $n = 9$ replicates. **** $P < 0.0001$.

b Proliferation assay of cells transduced with tandem repeats of the variant allele. Cells harboring eight tandem repeats proliferate significantly faster than cells harboring four tandem repeats, and cells harboring four tandem repeats proliferate significantly faster than cells harboring two or one repeat. Data are expressed as mean fold change of the cell line in the day seeded, \pm s.e.m., $n = 9$ replicates. **** $P < 0.0001$. All P -values were calculated with unpaired t -test

SPORE ($n = 105$), Memorial Sloan Kettering Lymphoproliferative Disorders Study (MSKCC)⁶² ($n = 64$), and ten additional studies^{11,12} (Supplementary Table 1). Among these 313 cases, 24 had a family history of a hematologic malignancy and 105 reported no family history; family history information was reported as unknown or was unavailable for the remainder. The stage 2 controls ($n = 564$) were obtained from Mayo CC/Iowa-Mayo SPORE ($n = 167$), MSKCC ($n = 302$),

and eight other studies^{11,12} (Supplementary Table 1). Characteristics of the replication population are shown in Supplementary Table 2.

SNP selection for replication. After ranking the SNPs by *P*-value and filtering for linkage disequilibrium (LD; $r^2 < 0.05$), we selected eleven SNPs from the most promising loci identified in stage 1 after imputation with $P < 5 \times 10^{-6}$ (Supplementary Table 6) for de novo replication in an independent sample of 313 WM/LPL unrelated cases and 564 controls. We chose the most significant imputed and genotyped SNPs at our two top loci (chromosome 6p25.3 and chromosome 14q32.13) and, whenever possible, the most significant SNP (genotyped or imputed) for additional promising loci with $P < 1 \times 10^{-6}$ in the discovery. Imputed SNPs with an information score ≤ 0.75 were excluded. Furthermore, only SNPs with MAF > 1% were selected for replication, and no SNPs proceeded to replication if they occurred in regions where they appeared as singletons or obvious artifacts. Of the 11 SNPs selected for replication, five were directly genotyped and the remaining six were imputed in the discovery.

Replication genotyping and analysis. We conducted genotyping on independent case-control sets in three centers using custom genotyping assays developed for either TaqMan (Applied Biosystems; validated at the NCI CGR) or Sequenom (Sequenom Laboratories; validated at the Mayo Clinic and MSKCC), or Sanger sequencing (for a single SNP, rs117410836, for which a custom TaqMan assay could not be designed). Genotyping was performed by the NCI CGR, the Mayo Clinic and MSKCC and included duplicates for quality control. Following exclusions for genotyping failures and self-reported non-European ancestry, data for 313 cases and 564 controls remained for analysis (Supplementary Table 10). Association testing was conducted assuming a log-additive model, adjusting for age, sex, Ashkenazi ancestry, and genotyping center, which appeared to be an appropriate model for the top SNPs (Supplementary Table 11). The results from the discovery and replication were then combined using a fixed-effects meta-analysis method with inverse variance weighting based on the estimates and standard error from each stage.

Technical validation. Technical validation was conducted for all SNPs taken forward for replication on a subset of cases ($n = 213$) and controls ($n = 478$) from the discovery. Comparing genotype calls from Taqman assays or Sanger sequencing with genotyped or imputed data from the GWAS showed high concordance (>97%) for all SNPs. Concordance for both genome-wide significant SNPs (rs116446171 and rs117410836) and the secondary signal at chromosome 14 (rs179159) was >99% (Supplementary Table 7).

Assessment of enrichment among high-risk families. Of the 122 WM/LPL cases in this study reporting a family history, 100 were enrolled in a family study of WM. Among these cases, 21 had the risk variant at rs116446171 or rs117410836 and at least one living relative diagnosed with a relevant B-cell disorder and DNA available for genotyping. To assess whether the risk variants occurred at a higher frequency than expected within high-risk families, we genotyped available affected relatives using the Illumina OmniExpress. After employing rigorous quality control metrics, genotype data were available for 58 relatives, including 32 first-degree relatives and 14 more distantly related relatives with WM, IgM MGUS, or other lymphoproliferative disorders (Supplementary Table 8). For index cases carrying the effect variant at either locus, we computed the frequency with which their affected relatives carried the same effect variant and used the binomial test to determine whether the frequency was greater than expected under the assumption that 50% of first-degree relatives would share the same variant.

Heritability analysis. To estimate the familial risk explained by these loci for WM/LPL, we estimated the contribution of each independent SNP to the heritability using the equation $h^2_{\text{SNP}} = \beta^2 2f(1-f)$, where β is the log-odds ratio per copy of the risk allele from the replication stage analyses and f is the allele frequency, and summed the contributions of all novel SNPs⁶³. We then estimated the total heritability based on the estimated relative risks = 24.0 and 20.0 in first-degree relatives for WM and WM/LPL, respectively, from Kristinsson et al.³ using the equation derived by Pharoah and colleagues⁶⁴. We calculated the proportion of familial risk explained by dividing the summed contributions of the novel SNPs by the total heritability. To estimate the contribution of all common SNPs to familial risk, we used the method proposed by Yang et al.⁶⁵ which was adapted to dichotomous traits⁶⁶ and implemented in the Genome-wide Complex Trait Analysis (GCTA) software (cns.genomics.com/software/gcta/). The genetic similarity matrix was estimated from our discovery scan using all genotyped autosomal SNPs with a minor allele frequency >0.01. We used restricted maximum likelihood (REML), the default option for GCTA, to fit the appropriate variance components model, assuming the lifetime risk of WM was 0.0003 to estimate heritability on a liability scale. We then transformed the obtained estimate into a sibling relative risk estimate and estimated the percentage of familial risk explained.

Functional annotation of rs116446171. To explore whether the rs116446171 SNP was encompassed within *EXOC2* transcripts in any cell type, we analyzed published

data from Poly(A)site (<http://www.polyasite.unibas.ch/>), an annotation tool build using a total of over 400 million reads from 78 3' end sequencing libraries generated with standard 3' end-sequencing protocols²². Poly(A) sites are annotated based on the protein-coding genes and long non-coding RNAs (lncRNAs) contained in the UCSC Basic Table of GENCODE V19. The original data and experimental methods are described by Lianoglou²¹. We analyzed data from the Genotype-Tissue Expression (GTEx) Project (<https://www.gtexportal.org/home/>) from whole blood, lymphocytes, and EBV-transformed lymphoblastoid cells to determine the presence of *cis* expression quantitative trait loci (eQTLs), adjusted for principal components. We explored possible effects of variation at rs116446171 on secondary RNA structure using RNAfold Server (<http://rna.tbi.univie.ac.at/cgi-bin/RNAWebSuite/RNAfold.cgi>), a thermodynamic structure prediction tool that predicts secondary minimum free energy structures and base pair probabilities from single RNA or DNA sequences²³. In parallel, these SNPs were compared to a collection of internally processed epigenetic data sets. Model-based analysis of ChIP-Seq (MACS) package⁶⁷ was used to identify H3K4me1, H3K4me3, and H3K27ac peaks from GSE50893 ChIP-seq data⁶⁸. Reference epigenome data was from the Roadmap Epigenomics Project (<http://www.roadmapepigenomics.org/>); other ChIP-seq and DNase-seq data were from the ENCODE project (<https://www.encodeproject.org/>). Signal tracks (reads per million) were generated using a 200-base pair (bp) sliding window and a step size of 20 bp. To determine potential SNP-gene promoter interactions, we used Capture Hi-C (<http://promoter.bx.psu.edu/hi-c/view.php>), a method for profiling chromosomal interactions involving targeted regions of interest, such as gene promoters, globally and at high resolution. We used promoter Capture Hi-C data in 17 primary hematopoietic cell types²³. Regions showing significant chromatin interactions with CHiCAGO (<http://regulatorygenomicsgroup.org/chicago>) scores ≥ 5 were downloaded from <https://osf.io/u8tzp/>.

Selection of SNP for functional evaluation. Our main finding, rs116446171, is located 679 bp downstream of the 3'UTR of the *EXOC2* gene. Although it is not predicted to be contained in any *EXOC2* transcript, we chose to further evaluate this SNP for possible functional relevance based on (1) prior evidence that this rs116446171 is also the most significant SNP associated with diffuse large B-cell lymphoma^{31,32}; (2) the unusually large observed effect size on WM/LPL risk; (3) in silico evidence suggesting an association with regulatory elements in primary B-cells and the lymphoblastoid cell line, GM12878; and (4) the observation that the risk variant might affect a predicted miRNA binding site.

Cell culture and generation of stable cell lines. HEK293T cells were used because of their reliable growth and transfection profile and suitability for gene expression analysis. HEK293T cells were obtained from American Type Culture Collection (293T ATCC® CRL-3216™; ATCC, Manassas, VA), where they were authenticated by Short Tandem Repeat (STR) profiling. The cells were maintained under standard cell culture conditions at 37 °C in 5% CO₂ in a humid environment. The culture medium, DMEM, was purchased from Mediatech Inc. (Manassas, VA) and supplemented with 10% FBS from Gemini Bio Products (West Sacramento, CA). Plasmocin Prophylactic (InvivoGen, San Diego, CA) was used in the culture medium to prevent mycoplasma contamination. Lentiviruses were produced by transfection of HEK293T packaging cells with a three plasmid system⁶⁹. To generate stable cell lines, HEK293T cells were seeded into 6-well plates for 24 h before infection with 5 multiplicity of infection (moi) of lentivirus in OptiMEM (Invitrogen; ThermoFisher Scientific, Waltham, MA) in the presence of 8 µg/mL polybrene (Sigma-Aldrich, Inc., St. Louis, MO). After the incubation, medium was replaced with fresh DMEM with 10% FBS for another 24 h before selection in medium containing 1 µg/mL of puromycin, until the control cells were no longer viable. All the stably transduced cell lines were subsequently maintained in medium supplemented with 0.5 µg/mL of puromycin during experimentation.

Plasmids and site-specific mutagenesis. The *EXOC2* 3'UTR Lenti-reporter-GFP (green fluorescent protein) vector was purchased from Applied Biological Materials Inc. (Richmond, BC, Canada Catalog # MT-h57118). To construct the reporter plasmids with the extended *EXOC2* 3'UTR containing the wild type, variant and deleted sequence (Supplementary Fig. 10a), a wild-type 987 bp fragment PCR-amplified with high Fidelity Platinum PCR SuperMix (Invitrogen) (forward 5'-GGCTTGTCAGGGTTTCAAG-3', reverse 5'-CATGCAAAGATGACAAGAGACG G-3') from human genomic DNA was first cloned into pCRII-TOPO (Invitrogen) and subsequently fused to the *EXOC2* 3'UTR Lenti-reporter-GFP vector with Choo-Choo cloning kit from MCLAB (South San Francisco, CA) to create the construct pCS-EGFP-3'C. For generation of the variant pCS-EGFP-3'G, PCR fragments (forward 5'-GTTGTAATTTACTTGACATTTTCCCT-3', reverse 5'-GTTAACTTGCTCCAGCTGCTGGTTT-3'; forward 5'-GTTAAACAACCCAGCACC TGGAGCA-3', reverse 5'-GCTGGAATGAAATGCCACT-3') were amplified with high Fidelity Platinum PCR SuperMix and used to replace the corresponding wild type fragment with Choo-Choo cloning kit. For generation of the deletion construct pCS-EGFP-3'Δ, PCR fragment (forward 5'-CTCGTAACTTCTCTCT CGGCTTTCATCTAAC-3', reverse 5'-GCTGGAATGAAATGCCACT-3') was amplified and replaced the corresponding wild type fragment with Choo-Choo cloning kit. To construct the empty vector, the commercial *EXOC2* 3'UTR

Lenti-reporter-GFP vector was digested with *EcoRI* and *XhoI* and re-ligated with Quick Blunting and Quick Ligation Kits from New England Biolabs (Ipswich, MA). For generation of the tandem repeats of a 25-bp sequence centered around rs116446171 C/G inserted into the *EcoRI* site of the extended *EXOC2* 3'UTR (Supplementary Fig. 10b), PCR primers (forward 5'-GTTAACTTGCTCCAGGTGCTGGTTT-3', reverse 5'-GTTAACAAACCAGCACCTGGAGCAA-3') were annealed and ligated into pCRII-TOPO with Quick Blunting and Quick Ligation Kits from New England Biolabs. Following digestion with *EcoRI*, fragments consisting of different tandem repeats were inserted into the *EcoRI* site of the *EXOC2* 3'UTR. All the clones with *cis* or *trans* orientation and various copy numbers of the tandem repeats were confirmed by sequencing performed by the Heflin Center for Genomic Sciences, University of Alabama at Birmingham.

Expression and normalization of pre-microRNAs. PremiR-378a-5p (Cat # mir-p227) and PremiR-324-3p (Cat # mir-p193) were expressed in self-inactivated (SIN) lentiviral, pLV-miR vectors purchased from BIOSETTA (San Diego, CA). The control vector (pLV13) was created by insertion of a 118-bp random sequence into the *XhoI* site of the pLV-miR vector (re-ligation of mir-p227 after deletion of the *XhoI* fragment containing the insert of miR-378a); 4 copies of the tandem repeats in *cis*-orientation were inserted into the *XhoI* site of the pLV-miRNA vector, which served as a locker plasmid (pLV18). All vectors express a pUro (red fluorescent puromycin-*N*-acetyl-transferase) gene and the measurement of the red fluorescence in cell lines after transfection can be used for normalization. Cells were transfected with the above constructs using lipofectamine to determine the effects of the microRNAs on the EGF reporter. The EGFP fluorescence was measured and normalized against transfection efficiencies in the same cell lines with different microRNA plasmids and normalized against the genomic copy number of EGFP among cell lines transduced with WT, Variant, Null, 3'UTR of *EXOC2* and vectors.

Cell proliferation assay. Live cells were enumerated at wavelength 570 nm using the MTT assay of mitochondrial enzymatic activity (CellTiter 96 Non-Radioactive Cell Proliferation Assay, Promega Corp., Madison, WI).

Real-time quantitative RT-PCR. Total RNA was extracted using the RNeasy Mini Kit (Qiagen, Louisville, KY) with on-column DNase digestion. Reverse transcription was performed with Accupower CycleScript RT Premix (Bioneer, Alameda, CA). Real-time quantitative PCR reactions were performed using SYBR green PCR Master Mix from Bio-Rad (Hercules, CA) with *EXOC2* primer (forward 5'-GATCCTTCAGCTCATGCACA-3', reverse 5'-GACTGAGATGGCCCAACACT-3') and EGFP primer (forward 5'-CAAGATCCGCCACAACATCG-3', reverse 5'-GACTGGGTGCTCAGGTAGTG-3'). Triplicate reactions for the genes of interest and 4 endogenous controls (ACTB, B2M, GAPDH, and GUSB) were performed separately on the same cDNA samples by using CFX Connect Real-Time System (Bio-Rad). Proprietary primer sets for ACTB, B2M, GAPDH, and GUSB were purchased from RealTimePrimers, LLC (<https://www.realtimprimers.com/>). The mean cycle threshold (C_t) was used for the $\Delta\Delta C_t$ computations of the relative transcript abundance.

Normalization for transduction efficiencies of cell lines. Genomic DNAs were purified with Quick-DNA Universal Kit (Zymo Research). Real-time quantitative PCR was performed using SYBR green PCR Master Mix with 3 sets of EGFP primer (Set I: forward 5'-CTTCTCAAGTCCGCCATG-3', reverse 5'-ATGTGATCGCGCTTCTCGTT-3'; Set II: forward 5'-CGTAAACGGCCACAAGTTCA-3', reverse 5'-CTTCATGTGGTCGGGGTAGC-3'; Set III forward 5'-CAAGATCCGCCACAACATCG-3', reverse 5'-GACTGGGTGCTCAGGTAGTG-3'), while GAPDH was used for the reference gene (Set I: forward 5'-CCCTTCATTGACCTCAACTACATGGT-3', reverse 5'-GAGGGCCATCCACAGCTTCTG-3'; Set II: forward 5'-GTGAAGGTCGGAGTCAACG-3', reverse 5'-TGAGGTCAATGAGGGGTC-3'). The ratio of copy number of the integrated reporter gene in cell lines was calculated against the reference gene GAPDH.

Direct measurement of EGFP and rPuro fluorescence. EGFP and rPuro fluorescence were measured directly with 6-well plates with or without Triton X-100 (1%) treatment using Synergy H1 Hybrid Reader (BioTek, Winooski, VT) Gen5 Microplate Reader and Imager Software (ex/em for GFP: 485/519 nm; for rPuro: 553/593 nm). Fluorescence measurements were performed using the bottom optic, orbital averaging with 2 mm diameter and 20 flashes per well. All the cell lines were cultured in the phenol red free DMEM media (Mediatech, Corning, NY) supplied with 10% FBS to lower the background. All measurements were background subtracted (HEK293T cells with no plasmid transfection) and normalized against the genomic copy number of the EGFP genes.

In silico miR-binding site prediction. miRBase (<http://www.mirbase.org/search.shtml>) homologous search with the wild type rs116446171 sequence detected significant homology with the mature microRNA, miR-378a-5p. rs116446171 sequence with a single C to G change eliminates that homology, and instead creates a new homology with the mature microRNA, miR-324-3p.

Statistical analysis for functional experiments. All the experimental data from cell viability and proliferation assays, EGFP reporter assay, and quantitative PCR analysis were performed by the unpaired *t*-test and fitted with an exponential growth equation of Prism 6 for Windows from GraphPad Software (San Diego CA). Data are shown as means \pm the standard error of the mean (s.e.m.) of values obtained for *n* replicates as indicated in the figure legends.

Disclaimer

The content of this publication does not necessarily reflect the views or policies of the Department of Health and Human Services, nor does mention of trade names, commercial products, or organizations imply endorsement by the U.S. Government.

Data availability

The genotyping dataset generated during this study has been deposited in the dbGaP repository with the accession code [phs001284.v1.p1](https://www.ncbi.nlm.nih.gov/geo/query/acc.cgi?acc=phs001284.v1.p1). All other relevant data generated for this study are available upon request from the authors.

Received: 17 November 2017 Accepted: 4 September 2018

Published online: 10 October 2018

References

- Swerdlow, S. H. et al. in *WHO Classification of Tumours of the Haematopoietic and Lymphoid Tissues* 4th edn (eds Swerdlow, S. H. et al.) (International Agency for Research on Cancer, Lyon, 2008).
- Teras, L. R. et al. 2016 US lymphoid malignancy statistics by World Health Organization subtypes. *CA Cancer J. Clin.* **66**, 443–459 (2016).
- Kristinsson, S. Y. et al. Risk of lymphoproliferative disorders among first-degree relatives of lymphoplasmacytic lymphoma/Waldenström macroglobulinemia patients: a population-based study in Sweden. *Blood* **112**, 3052–3056 (2008).
- Altieri, A., Bermejo, J. L. & Hemminki, K. Familial aggregation of lymphoplasmacytic lymphoma with non-Hodgkin lymphoma and other neoplasms. *Leukemia* **19**, 2342–2343 (2005).
- Koshiol, J., Gridley, G., Engels, E. A., McMaster, M. L. & Landgren, O. Chronic immune stimulation and subsequent Waldenström macroglobulinemia. *Arch. Intern. Med.* **168**, 1903–1909 (2008).
- Kristinsson, S. Y. et al. Immune-related and inflammatory conditions and risk of lymphoplasmacytic lymphoma or Waldenström macroglobulinemia. *J. Natl Cancer Inst.* **102**, 557–567 (2010).
- Royer, R. H. et al. Differential characteristics of Waldenström macroglobulinemia according to patterns of familial aggregation. *Blood* **115**, 4464–4471 (2010).
- Vajdic, C. M. et al. Medical history, lifestyle, family history, and occupational risk factors for lymphoplasmacytic lymphoma/Waldenström's macroglobulinemia: the InterLymph Non-Hodgkin Lymphoma Subtypes Project. *J. Natl Cancer Inst. Monogr.* **2014**, 87–97 (2014).
- Treon, S. P. et al. MYD88 L265P somatic mutation in Waldenström's macroglobulinemia. *N. Engl. J. Med.* **367**, 826–833 (2012).
- McMaster, M. L. et al. Genomewide linkage screen for Waldenström macroglobulinemia susceptibility loci in high-risk families. *Am. J. Hum. Genet.* **79**, 695–701 (2006).
- Berndt, S. I. et al. Genome-wide association study identifies multiple risk loci for chronic lymphocytic leukemia. *Nat. Genet.* **45**, 868–876 (2013).
- Berndt, S. I. et al. Two susceptibility loci identified for prostate cancer aggressiveness. *Nat. Commun.* **6**, 6889 (2015).
- Yang, J. et al. Genomic inflation factors under polygenic inheritance. *Eur. J. Hum. Genet.* **19**, 807–812 (2011).
- McCarthy, S. et al. A reference panel of 64,976 haplotypes for genotype imputation. *Nat. Genet.* **48**, 1279–1283 (2016).
- Helbig, I., Hodge, S. E. & Ottman, R. Familial cosegregation of rare genetic variants with disease in complex disorders. *Eur. J. Hum. Genet.* **21**, 444–450 (2013).
- Javierre, B. M. et al. Lineage-specific genome architecture links enhancers and non-coding disease variants to target gene promoters. *Cell* **167**, 1369–1384 (2016).
- Mifsud, B. et al. Mapping long-range promoter contacts in human cells with high-resolution capture Hi-C. *Nat. Genet.* **47**, 598–606 (2015).
- Jin, F. et al. A high-resolution map of the three-dimensional chromatin interactome in human cells. *Nature* **503**, 290–294 (2013).
- Mayr, C. Regulation by 3'-untranslated regions. *Ann. Rev. Genet.* **51**, 171–194 (2017).
- Singh, I. et al. Widespread intronic polyadenylation diversifies immune cell transcriptomes. *Nat. Commun.* **9**, 1716 (2018).

21. Lianoglou, S., Garg, V., Yang, J. L., Leslie, C. S. & Mayr, C. Ubiquitously transcribed genes use alternative polyadenylation to achieve tissue-specific expression. *Genes Dev.* **27**, 2380–2396 (2013).
22. Gruber, A. J. et al. A comprehensive analysis of 3' end sequencing data sets reveals novel polyadenylation signals and the repressive role of heterogeneous ribonucleoprotein C on cleavage and polyadenylation. *Genome Res.* **26**, 1145–1159 (2016).
23. Hofacker, I. L. Vienna RNA secondary structure server. *Nucleic Acids Res.* **31**, 3429–3431 (2003).
24. Cerami, E. et al. The cBio cancer genomics portal: an open platform for exploring multidimensional cancer genomics data. *Cancer Discov.* **2**, 401–404 (2012).
25. Forbes, S. A. et al. COSMIC: somatic cancer genetics at high-resolution. *Nucleic Acids Res.* **45**, D777–D783 (2017).
26. Lee, D. Y., Deng, Z., Wang, C.-H. & Yang, B. B. MicroRNA-378 promotes cell survival, tumor growth, and angiogenesis by targeting SuFu and Fus-1 expression. *Proc. Natl Acad. Sci. USA* **104**, 20350–20355 (2007).
27. Kuo, W. T. et al. MicroRNA-324 in human cancer: miR-324-5p and miR-324-3p have distinct biological functions in human cancer. *Anticancer Res.* **36**, 5189–5196 (2016).
28. Dharap, A., Pokrzywa, C., Murali, S., Pandi, G. & Vemuganti, R. MicroRNA miR-324-3p induces promoter-mediated expression of RelA gene. *PLoS ONE* **8**, e79467 (2013).
29. Nagel, D., Vincendiau, M., Eitelhuber, A. C. & Krappmann, D. Mechanisms and consequences of constitutive NF- κ B activation in B-cell lymphoid malignancies. *Oncogene* **33**, 5655–5665 (2014).
30. Yang, G. et al. A mutation in MYD88 (L265P) supports the survival of lymphoplasmacytic cells by activation of Bruton tyrosine kinase in Waldenström macroglobulinemia. *Blood* **122**, 1222–1232 (2013).
31. Cerhan, J. R. et al. Genome-wide association study identifies multiple susceptibility loci for diffuse large B cell lymphoma. *Nat. Genet.* **46**, 1233–1238 (2014).
32. Bassig, B. A. et al. Genetic susceptibility to diffuse large B-cell lymphoma in a pooled study of three Eastern Asian populations. *Eur. J. Haematol.* **95**, 442–448 (2015).
33. De Silva, N. S., Simonetti, G., Heise, N. & Klein, U. The diverse roles of IRF4 in late germinal center B-cell differentiation. *Immunol. Rev.* **247**, 73–92 (2012).
34. Feldman, A. L. et al. Discovery of recurrent t(6;7)(p25.3;q32.3) translocations in ALK-negative anaplastic large cell lymphomas by massively-parallel genomic sequencing. *Blood* **117**, 915–919 (2011).
35. Shukla, V., Ma, S., Hardy, R. R., Joshi, S. S. & Lu, R. A role for IRF4 in the development of CLL. *Blood* **122**, 2848–2855 (2013).
36. Gutiérrez, N. C. et al. Gene expression profiling of B lymphocytes and plasma cells from Waldenström's macroglobulinemia: comparison with expression patterns of the same cell counterparts from chronic lymphocytic leukemia, multiple myeloma and normal individuals. *Leukemia* **21**, 541–549 (2007).
37. Roberts, M. J. et al. Nuclear protein dysregulation in lymphoplasmacytic lymphoma/Waldenström macroglobulinemia. *Hematopathol.* **139**, 210–219 (2013).
38. Ochiai, K. et al. Transcriptional regulation of germinal center B and plasma cell fates by dynamical control of IRF4. *Immunity* **38**, 918–929 (2013).
39. Negishi, H. et al. Negative regulation of Toll-like-receptor signaling by IRF4. *Proc. Natl Acad. Sci. USA* **102**, 15989–15994 (2005).
40. Lang, R., Hammer, M. & Mages, J. DUSP meet immunology: dual specificity MAPK phosphatases in control of the inflammatory response. *J. Immunol.* **177**, 7497–7504 (2006).
41. Sekine, Y. et al. Regulation of STAT3-mediated signaling by LMW-DSP2. *Oncogene* **25**, 5801–5806 (2006).
42. Fulciniti, M. et al. MYD88-independent growth and survival effects of Sp1 transactivation in Waldenström macroglobulinemia. *Blood* **123**, 2673–2681 (2014).
43. Ishikawa, H., Ma, Z. & Barber, G. N. STING regulates intracellular DNA-mediated, type I interferon-dependent innate immunity. *Nature* **461**, 788–793 (2009).
44. Kashatus, D. F. Ral GTPases in tumorigenesis: emerging from the shadows. *Exp. Cell Res.* **319**, 2337–2342 (2013).
45. Bodemann, B. O. & White, M. A. Ral GTPases and cancer: linchpin support of the tumorigenic platform. *Nat. Rev. Cancer* **8**, 133–140 (2008).
46. Chien, Y. et al. RalB GTPase-mediated activation of the I κ B family kinase TBK1 couples innate immune signaling to tumor cell survival. *Cell* **127**, 157–170 (2006).
47. Adams, B. D., Anastasiadou, E., Esteller, M., He, L. & Slack, F. J. The inescapable influence of noncoding RNAs in cancer. *Cancer Res.* **75**, 5206–5210 (2015).
48. Rapicavoli, N. A. et al. A mammalian pseudogene lncRNA at the interface of inflammation and anti-inflammatory therapeutics. *eLife* **2**, e00762 (2013).
49. Huang, W. et al. DDX5 and its associated lncRNA Rmrp modulate TH17 cell effector functions. *Nature* **528**, 517–522 (2015).
50. Carpenter, S. et al. A long noncoding RNA mediates both activation and repression of immune response genes. *Science* **341**, 789–792 (2013).
51. Lemal, R. et al. TCL1 expression patterns in Waldenström macroglobulinemia. *Mod. Pathol.* **29**, 83–88 (2016).
52. Hoyer, K. K. et al. Dysregulated TCL1 promotes multiple classes of mature B cell lymphoma. *Proc. Natl Acad. Sci. USA* **99**, 14392–14397 (2002).
53. Laine, J., Künstle, G., Obata, T., Sha, M. & Noguchi, M. The protooncogene *TCL1* is an Akt kinase coactivator. *Mol. Cell* **6**, 395–407 (2000).
54. Ropars, V. et al. The TCL1A oncoprotein interacts directly with the NF- κ B inhibitor I κ B. *PLoS ONE* **4**, e6567 (2009).
55. Gaudio, E. et al. Tc1 interacts with Atm and enhances NF- κ B activation in hematologic malignancies. *Blood* **119**, 180–187 (2012).
56. Zhou, W. et al. Mosaic loss of chromosome Y is associated with common variation near *TCL1A*. *Nat. Genet.* **48**, 563–568 (2016).
57. Turner, J. J. et al. InterLymph hierarchical classification of lymphoid neoplasms for epidemiologic research based on the WHO classification (2008): update and future directions. *Blood* **116**, e90–e98 (2010).
58. Yu, K. et al. Population substructure and control selection in genome-wide association studies. *PLoS ONE* **3**, e2551 (2008).
59. Pritchard, J. K., Stephens, M. & Donnelly, P. Inference of population structure using multilocus genotype data. *Genetics* **155**, 945–959 (2000).
60. International HapMap Consortium et al. A second generation human haplotype map of over 3.1 million SNPs. *Nature* **449**, 851–861 (2007).
61. Price, A. L. et al. Principal components analysis corrects for stratification in genome-wide association studies. *Nat. Genet.* **38**, 904–909 (2006).
62. Vijai, J. et al. Susceptibility loci associated with specific and shared subtypes of lymphoid malignancies. *PLoS Genet.* **9**, e1003220 (2013).
63. Park, J. H. et al. Estimation of effect size distribution from genome-wide association studies and implications for future discoveries. *Nat. Genet.* **42**, 570–575 (2010).
64. Pharoah, P. D. et al. Polygenic susceptibility to breast cancer and implications for prevention. *Nat. Genet.* **31**, 33–36 (2002).
65. Yang, J. et al. Common SNPs explain a large proportion of the heritability for human height. *Nat. Genet.* **42**, 565–569 (2010).
66. Lee, S. H., Wray, N. R., Goddard, M. E. & Visscher, P. M. Estimating missing heritability for disease from genome-wide association studies. *Am. J. Hum. Genet.* **88**, 294–305 (2011).
67. Zhang, Y. et al. Model-based analysis of ChIP-Seq (MACS). *Genome Biol.* **9**, R137 (2008).
68. Kasowski, M. et al. Extensive variation in chromatin states across humans. *Science* **342**, 750–752 (2013).
69. Falahati, R. et al. Chemoselection of allogeneic HSC after murine neonatal transplantation without myeloablation or post-transplant immunosuppression. *Mol. Ther.* **20**, 2180–2189 (2012).

Acknowledgements

We wish to thank Seth A. Brodie, PhD, for his critical reading of the manuscript and his intellectual contributions to the functional experimental approach. The Genotype-Tissue Expression (GTEx) Project was supported by the Common Fund of the Office of the Director of the National Institutes of Health, and by NCI, NHGRI, NHLBI, NIDA, and NINDS. The data used for the analyses described in this manuscript were obtained from the GTEx Portal on 03/07/2018. This project has been funded in whole or in part with federal funds from the National Cancer Institute, National Institutes of Health, under Contract No. HHSN261200800001E. Further acknowledgements are provided in Supplementary Note 1.

Author contributions

M.L.M., S.I.B., J.Z., S.L.S., R.M., C.L., S.J.C., N.R., J.V., L.R.G., C.F.S., and N.E.C. designed and/or organized the study. M.L.M., S.I.B., S.L.S., L.B., B.D.H., A.H., M.Y., K.O., J.R.C., S.J.C., J.V., and N.E.C. conducted and/or supervised the genotyping. M.L.M., S.I.B., J.Z., S.A.L., B.Z., C.C.C., J.P., Z.W., and N.C. contributed to the statistical analysis. M.L.M., S.I.B., J.Z., S.L.S., S.A.L., C.M.V., K.E.S., G.K., E.E.B., A.Sm., J.R.C., S.J.C., N.R., J.V., L.R.G., C.F.S., and N.E.C. participated in the working group and/or writing the first draft. J.Z., A.I.O., J.R., H.Y., M.M.F., C.M., J.V., and C.F.S. designed, conducted and/or supervised experiments for the functional and phenotypic characterization of *EXOC2* risk variants. M.L.M., S.I.B., S.L.S., C.M.V., K.E.S., B.M.B., L.R.T., H.O.A., P.M.B. J.M., A.Mo., B.K.L., R.C.H.V., S.M.A., A.Ma., W.R.D., M.Me., P.K., P.B., J.C., E.G., C.M.B., F.C., R.C.T., P.V., E.W., N.B., Y.B., P.B., L.F., M.Ma., A.N., S.d.S., A.St., L.C., B.G., H.H., N.P., A.L.F., A.J.N., B.B., Q.L., T.Z., K.E.N., L.F.T., W.C., R.K.S., J.H., Y.Z., R.D.J., L.M.M., M.P.P., K.O., J.R.C., N.R., J.V., L.R.G., C.F.S., and N.E.C. conducted epidemiologic studies and contributed samples to the GWAS and/or replication. All authors read and approved the manuscript.

Additional information

Supplementary Information accompanies this paper at <https://doi.org/10.1038/s41467-018-06541-2>.

Competing interests: The authors declare no competing interests.

Reprints and permission information is available online at <http://npg.nature.com/reprintsandpermissions/>

Publisher's note: Springer Nature remains neutral with regard to jurisdictional claims in published maps and institutional affiliations.



Open Access This article is licensed under a Creative Commons Attribution 4.0 International License, which permits use, sharing, adaptation, distribution and reproduction in any medium or format, as long as you give appropriate credit to the original author(s) and the source, provide a link to the Creative Commons license, and indicate if changes were made. The images or other third party material in this article are included in the article's Creative Commons license, unless indicated otherwise in a credit line to the material. If material is not included in the article's Creative Commons license and your intended use is not permitted by statutory regulation or exceeds the permitted use, you will need to obtain permission directly from the copyright holder. To view a copy of this license, visit <http://creativecommons.org/licenses/by/4.0/>.

© The Author(s) 2018

Mary L. McMaster¹, Sonja I. Berndt¹, Jianqing Zhang², Susan L. Slager³, Shengchao Alfred Li⁴, Claire M. Vajdic⁵, Karin E. Smedby^{6,7}, Huihuang Yan³, Brenda M. Birmann⁸, Elizabeth E. Brown⁹, Alex Smith¹⁰, Geffen Kleinstern³, Mervin M. Fansler^{11,12}, Christine Mayr¹², Bin Zhu⁴, Charles C. Chung⁴, Ju-Hyun Park¹³, Laurie Burdette⁴, Belynda D. Hicks⁴, Amy Hutchinson⁴, Lauren R. Teras¹⁴, Hans-Olov Adami^{15,16,17}, Paige M. Bracci¹⁸, James McKay¹⁹, Alain Monnereau^{20,21,22}, Brian K. Link²³, Roel C.H. Vermeulen^{24,25}, Stephen M. Ansell²⁶, Ann Maria²⁷, W. Ryan Diver¹⁴, Mads Melbye^{28,29}, Akinyemi I. Ojesina², Peter Kraft^{16,30}, Paolo Boffetta³¹, Jacqueline Clavel^{20,21}, Edward Giovannucci^{8,16,32}, Caroline M. Besson³³, Federico Canzian³⁴, Ruth C. Travis³⁵, Paolo Vineis^{36,37}, Elisabete Weiderpass^{15,38,39,40}, Rebecca Montalvan⁴¹, Zhaoming Wang^{42,43}, Meredith Yeager⁴, Nikolaus Becker⁴⁴, Yolanda Benavente^{45,46}, Paul Brennan¹⁹, Lenka Foretova⁴⁷, Marc Maynadie⁴⁸, Alexandra Nieters⁴⁹, Silvia de Sanjose^{45,46}, Anthony Staines⁵⁰, Lucia Conde⁵¹, Jacques Riby^{2,52}, Bengt Glimelius⁵³, Henrik Hjalgrim^{28,54}, Nisha Pradhan²⁷, Andrew L. Feldman⁵⁵, Anne J. Novak²⁶, Charles Lawrence⁴¹, Bryan A. Bassig¹, Qing Lan¹, Tongzhang Zheng⁵⁶, Kari E. North^{57,58}, Lesley F. Tinker⁵⁹, Wendy Cozen^{60,61}, Richard K. Severson⁶², Jonathan N. Hofmann¹, Yawei Zhang⁶³, Rebecca D. Jackson⁶⁴, Lindsay M. Morton¹, Mark P. Purdue^{1,65}, Nilanjan Chatterjee^{1,66,67}, Kenneth Offit²⁷, James R. Cerhan³, Stephen J. Chanock¹, Nathaniel Rothman¹, Joseph Vijai²⁷, Lynn R. Goldin¹, Christine F. Skibola⁶⁸ & Neil E. Caporaso¹

¹Division of Cancer Epidemiology and Genetics, National Cancer Institute, Bethesda 20892 MD, USA. ²Department of Epidemiology, School of Public Health and Comprehensive Cancer Center, University of Alabama at Birmingham, Birmingham 35233 AL, USA. ³Department of Health Sciences Research, Mayo Clinic, Rochester 55905 MN, USA. ⁴Cancer Genomics Research Laboratory, Leidos Biomedical Research, Inc., Frederick National Lab for Cancer Research, Frederick 20877 MD, USA. ⁵Centre for Big Data Research in Health, University of New South Wales, Sydney 2052 NSW, Australia. ⁶Department of Medicine, Solna Karolinska Institutet, Stockholm 17176, Sweden. ⁷Hematology Center, Karolinska University Hospital, Stockholm 17176, Sweden. ⁸Channing Division of Network Medicine, Department of Medicine, Brigham and Women's Hospital and Harvard Medical School, Boston 02115 MA, USA. ⁹Department of Pathology, University of Alabama at Birmingham, Birmingham 35233 AL, USA. ¹⁰Department of Health Sciences, University of York, York YO10 5DD, UK. ¹¹Tri-Institutional Training Program in Computational Biology and Medicine, Weill Cornell Graduate College, New York 10021 NY, USA. ¹²Cancer Biology and Genetics Program, Memorial Sloan Kettering Cancer Center, New York 10065 NY, USA. ¹³Department of Statistics, Dongguk University, Seoul 100-715, Republic of Korea. ¹⁴Epidemiology Research Program, American Cancer Society, Atlanta 30303 GA, USA. ¹⁵Department of Medical Epidemiology and Biostatistics, Karolinska Institutet, Stockholm 17177, Sweden. ¹⁶Department of Epidemiology, Harvard T.H. Chan School of Public Health, Boston 02115 MA, USA. ¹⁷Institute of Health and Society, Clinical Effectiveness Research Group, University of Oslo, Oslo NO-0316, Norway. ¹⁸Department of Epidemiology and Biostatistics, University of California, San Francisco, San Francisco 94118 CA, USA. ¹⁹International Agency for Research on Cancer (IARC), Lyon 69372, France. ²⁰Epidemiology of Childhood and Adolescent Cancers Group, Inserm, Center of Research in Epidemiology and Statistics Sorbonne Paris Cité (CRESS), Paris F-94807, France. ²¹Université Paris Descartes, Paris 75006, France. ²²Registry of Hematological Malignancies in Gironde, Institut Bergonié, University of Bordeaux, Inserm, Team EPICENE, UMR 1219, Bordeaux 33000, France. ²³Department of Internal Medicine, Carver College of Medicine, The University of Iowa, Iowa City 52242 IA, USA. ²⁴Institute for Risk Assessment Sciences, Utrecht University, Utrecht 3508 TD, The Netherlands. ²⁵Julius Center for Health Sciences and Primary Care, University Medical Center Utrecht, Utrecht 3584 CX, The Netherlands. ²⁶Department of Internal Medicine, Mayo Clinic, Rochester 55905 MN, USA. ²⁷Department of Medicine, Memorial Sloan Kettering Cancer Center, New York 10065 NY, USA. ²⁸Division of Health Surveillance and Research, Department of Epidemiology Research, Statens Serum Institut, Copenhagen 2300, Denmark. ²⁹Department of Medicine, Stanford University School of Medicine, Stanford 94305 CA, USA. ³⁰Department of

Biostatistics, Harvard T.H. Chan School of Public Health, Boston 02115 MA, USA. ³¹The Tisch Cancer Institute, Icahn School of Medicine at Mount Sinai, New York 10029 NY, USA. ³²Department of Nutrition, Harvard T.H. Chan School of Public Health, Boston 02115 MA, USA. ³³Service d'hématologie et Oncologie, Centre Hospitalier de Versailles, Le Chesnay, Inserm U1018, Centre pour la Recherche en Epidémiologie et Santé des Populations (CESP), Villejuif 78157, France. ³⁴Genomic Epidemiology Group, German Cancer Research Center (DKFZ), Heidelberg 69120, Germany. ³⁵Cancer Epidemiology Unit, University of Oxford, Oxford OX3 7LF, UK. ³⁶MRC-PHE Centre for Environment and Health, School of Public Health, Imperial College London, London W2 1PG, UK. ³⁷Human Genetics Foundation, Turin 10126, Italy. ³⁸Department of Community Medicine, Faculty of Health Sciences, University of Tromsø, The Arctic University of Norway, Tromsø 9019, Norway. ³⁹Department of Research, Cancer Registry of Norway, Institute of Population-Based Cancer Research, Oslo 0379, Norway. ⁴⁰Genetic Epidemiology Group, Folkhälsan Research Center and University of Helsinki, Helsinki 00250, Finland. ⁴¹Westat, Rockville 20850 MD, USA. ⁴²Department of Computational Biology, St. Jude Children's Research Hospital, Memphis 38105 TN, USA. ⁴³Laboratory of Translational Genomics, Division of Cancer Epidemiology and Genetics, National Cancer Institute, Bethesda 20877 MD, USA. ⁴⁴Division of Cancer Epidemiology, German Cancer Research Center (DKFZ), Heidelberg 69120 Baden-Württemberg, Germany. ⁴⁵Cancer Epidemiology Research Programme, Catalan Institute of Oncology-IDIBELL, L'Hospitalet de Llobregat, Barcelona 08908, Spain. ⁴⁶CIBER Epidemiología y Salud Pública (CIBERESP), Madrid 28029, Spain. ⁴⁷Department of Cancer Epidemiology and Genetics, Masaryk Memorial Cancer Institute and MF MU, Brno 65653, Czech Republic. ⁴⁸EA 4184, Registre des Hémopathies Malignes de Côte d'Or, University of Burgundy and Dijon University Hospital, Dijon 21070, France. ⁴⁹Center for Chronic Immunodeficiency, University Medical Center Freiburg, Freiburg 79108 Baden-Württemberg, Germany. ⁵⁰School of Nursing and Human Sciences, Dublin City University, Dublin 9, Ireland. ⁵¹Bill Lyons Informatics Centre, UCL Cancer Institute, University College London, London WC1E 6DD, UK. ⁵²Division of Environmental Health Sciences, University of California Berkeley School of Public Health, Berkeley 94720 CA, USA. ⁵³Department of Immunology, Genetics and Pathology, Uppsala University, Uppsala 75105, Sweden. ⁵⁴Department of Hematology, Rigshospitalet, Copenhagen 2100, Denmark. ⁵⁵Department of Laboratory Medicine and Pathology, Mayo Clinic, Rochester 55905 MN, USA. ⁵⁶Department of Epidemiology, Brown University, Providence 02903 RI, USA. ⁵⁷Department of Epidemiology, University of North Carolina at Chapel Hill, Chapel Hill 27599 NC, USA. ⁵⁸Carolina Center for Genome Sciences, University of North Carolina at Chapel Hill, Chapel Hill 27599 NC, USA. ⁵⁹Division of Public Health Sciences, Fred Hutchinson Cancer Research Center, Seattle 98117 WA, USA. ⁶⁰Department of Preventive Medicine, USC Keck School of Medicine, University of Southern California, Los Angeles 90033 CA, USA. ⁶¹Norris Comprehensive Cancer Center, USC Keck School of Medicine, University of Southern California, Los Angeles 90033 CA, USA. ⁶²Department of Family Medicine and Public Health Sciences, Wayne State University, Detroit 48201 MI, USA. ⁶³Department of Environmental Health Sciences, Yale School of Public Health, New Haven 06520 CT, USA. ⁶⁴Division of Endocrinology, Diabetes and Metabolism, The Ohio State University, Columbus 43210 OH, USA. ⁶⁵Ontario Health Study, Toronto M5S 1C6 ON, Canada. ⁶⁶Department of Biostatistics, Bloomberg School of Public Health, Johns Hopkins University, Baltimore 21205 MD, USA. ⁶⁷Department of Oncology, School of Medicine, Johns Hopkins University, Baltimore 21205 MD, USA. ⁶⁸Department of Hematology and Medical Oncology, Emory University School of Medicine, Atlanta 30322 GA, USA. These authors contributed equally: Mary L. McMaster, Sonja I. Berndt, Jianqing Zhang, Susan L. Slager. These authors jointly supervised this work: Stephen J. Chanock, Nathaniel Rothman, Joseph Vijai, Lynn R. Goldin, Christine F. Skibola, Neil E. Caporaso.